Front. Mech. Eng. 2012, 7(4): 357–370
DOI 10.1007/s11465-012-0340-5

RESEARCH ARTICLE

Conghui LIANG, Marco CECCARELLI, Yukio TAKEDA

Operation analysis of a Chebyshev-Pantograph leg mechanism for a single DOF biped robot

Abstract In this paper, operation analysis of a Chebyshev-Pantograph leg mechanism is presented for a single degree of freedom (DOF) biped robot. The proposed leg mechanism is composed of a Chebyshev four-bar linkage and a pantograph mechanism. In contrast to general fully actuated anthropomorphic leg mechanisms, the proposed leg mechanism has peculiar features like compactness, low-cost, and easy-operation. Kinematic equations of the proposed leg mechanism are formulated for a computer oriented simulation. Simulation results show the operation performance of the proposed leg mechanism with suitable characteristics. A parametric study has been carried out to evaluate the operation performance as function of design parameters. A prototype of a single DOF biped robot equipped with two proposed leg mechanisms has been built at LARM (Laboratory of Robotics and Mechatronics). Experimental test shows practical feasible walking ability of the prototype, as well as drawbacks are discussed for the mechanical design.

Keywords biped robots, leg mechanisms, simulation

1 Introduction

It is well known that legged locomotion is more efficient, speedy, and versatile than the one by track and wheeled vehicles when it operates on a rough terrain, it is used to climb stairs or to avoid obstacles [1,2]. This research field has attracted great interests in the past decades and a lot of prototypes have been successfully built in the university laboratories or companies. They have been often presented in CLAWAR conferences. Walking abilities are achieved for dynamic walking, ascending and descending stairs, passive dynamic walking, running, and even jumping. Significant examples can be indicated in the biped humanoid robot HRP-2 as developed by AIST [3], WABIAN-II biped humanoid robot at the Takanishi laboratory [4], and Honda's ASIMO [5].

Most of research projects on biped walking robots are on the aspects of dynamic walking control, walking pattern generation, and human-robot interaction. Nevertheless, mechanism design of biped robots, especially for leg mechanisms, is still a crucial issue to build efficient and reliable biped robots. A leg mechanism will not only determine the degrees of freedom of a robot, but also actuation system efficiency and its control strategy. Therefore, leg mechanisms are fundamental for design and operation issues in a biped walking robot design as pointed out in Refs. [1,2].

In order to make a biped robot walking anthropomorphic like, most of the leg mechanisms are build with an anthropomorphic architecture with three actuating motors at least at the hip, knee, and ankle. These kinds of leg mechanisms have an anthropomorphic design, and therefore they show anthropomorphic flexible motion capability. However, there are several drawbacks, namely the leg system design is very complex, difficult, and expensive when considering the number of motors and their proper distribution. Because of the natural static unstable characters, sophisticated control algorithms and electronics hardware are also needed. In addition, they are not energy efficient because of the "Back-driven" effect (as it is known the force conflict between different motors when a leg swings) and heavy masses of motors with gear boxes [1]. Thus, it is very difficult to build properly a biped robot with those leg mechanisms, as well as to operate biped robot walking in a real environment for some tasks.

A different methodology can be considered such as constructing a biped robot with reduced number of degrees of freedom and compact mechanical design. Therefore,

Received July 10, 2012; accepted August 25, 2012

Conghui LIANG, Marco CECCARELLI (✉)
Laboratory of Robotics and Mechatronics, University of Cassino and South Latium, Cassino 03043, Italy
E-mail: ceccarelli@unicas.it

Yukio TAKEDA
Department of Mechanical Sciences and Engineering, Tokyo Institute of Technology, Tokyo 152-8552, Japan

careful attention can be paid on a mechanism design of the leg system and actuation system. Characters such as mechanism dimension, workspace, actuating torque can be considered and optimized in a novel leg design.

Actually, the concept of reduced DOF leg mechanisms design has been used since hundreds of years ago, like the wooden ox and gliding horse in ancient China [6], the wooden horse of Rygg in 1893 [1], and Chebyshev walking machines [7]. Most of such kinds of leg mechanisms are successfully applied in four-legged or six-legged robots as listed for example in Ref. [2]. Several prototypes have high efficiency with reduced DOF leg mechanisms like for example ASV, OSU, PVII, and ODEX [1]. Mechanism design and optimization problems for different kinds of leg mechanisms are studied extensively, like for examples in Refs. [8,9]. In Refs. [10,11], a walking chair is proposed as an alternative vehicle to a wheelchair and it is based on leg mechanisms as an application for welfare facilities.

At LARM, Laboratory of Robotics and Mechatronics in the University of Cassino, a research line is directed to the low-cost easy-operation leg mechanism design. Several prototypes have been built with reduced DOF leg mechanisms for biped robots [12] and for a rickshaw walking robot [13]. This leg mechanism has been also investigated to be applied even in a low-cost easy-operation humanoid robot namely CALUMA [14].

In this paper, a single DOF leg mechanism with linkage architecture has been proposed. Kinematic equations are formulated and the dynamic operation performance of the leg mechanism has been investigated by numerical simulation. Simulation and experimental tests show feasible operation performance of the proposed leg mechanism as well as the overall design for a single DOF biped robot. Finally, a parametric study has been carried out to evaluate the operation performance as function of the design parameters.

2 Mechanism description

For human normal walking, the motion of a leg can be divided into two phases, namely a propelling phase and non-propelling phase [2]. In Fig. 1 the dashed line represents the supporting leg in propelling phase and the solid line represents the swinging leg in non-propelling phase. Each leg operates in these two phases sequentially by propelling the human body forward. Particularly, a short period of double supporting phase exists when two legs are in contact with the ground at the same time. The motion trajectory of the ankle point is indicated with dashed line and it is a symmetric curve. The hip trajectory is a quasi sinusoid shaped curve [15]. The walking gait is characterized by the step length L and step height H as indicated in Fig. 1.

Therefore, in order to design a leg mechanism with rear-

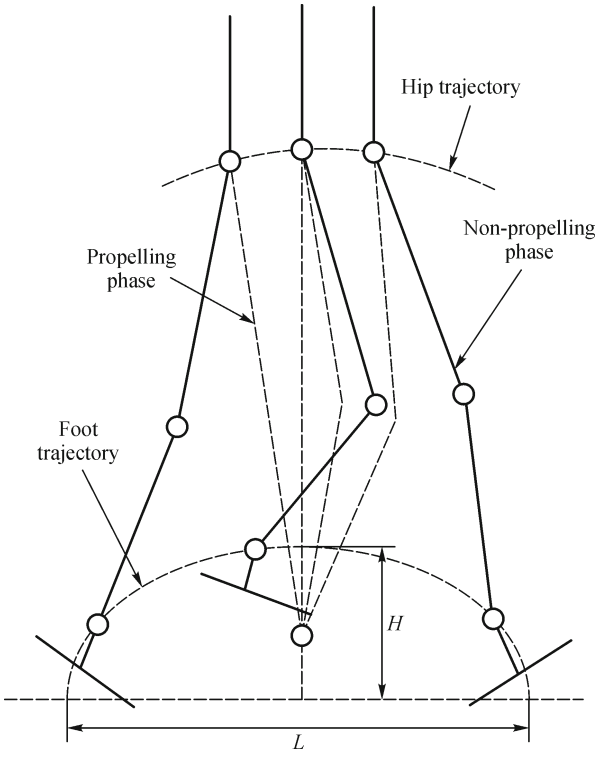

Fig. 1 Scheme of human walking gait with its main parameters

forth and up-down motion capability in sagittal plane with only one actuation motor, the foot point of a leg mechanism must be able to trace an ovoid curve, which is composed of a straight-line segment and a curved segment. The straight-line segment is related to the propelling phase when the corresponding leg is in contact with the ground and it must guarantee a stable propelling of the body. The curved segment is related to the non-propelling phase, which is produced by leg when it swings from rear to forth.

Mechanisms, which can produce coupler curves with a straight-line segment motion, are studied intensively in a very rich literature. There are very famous mechanisms, like for example the four-bar linkages that have been conceived by Watt James, Oliver Evans, Richard Roberts, and Pafnuty Chebyshev. They are reported in many textbooks and mechanisms catalogues, like for example in Refs. [16,17]. In addition, alternative mechanisms have been also investigated with many complex solutions [7]. In the work [18] four-bar linkages, six-bar linkages, and eight-bar linkages are classified and selected in order to find a proper mechanism structure, which is able to produce an ovoid curve with an approximate straight-line segment. The Funabashi single DOF biped walking machine consists two six-bar linkages, where an adjustable mechanism with variable crank length has been proposed [19] and the mechanism synthesis problem has been studied with a six-bar dwell mechanism as leg mechanism for a biped robot. The synthesis problem is presented in

Refs. [20,21] by considering the workspace and static characteristics of the pantograph mechanism.

A Chebyshev four-bar linkage design is considered here because of its simplicity and characteristics [22]. In order to reduce the dimension of the leg mechanism a pantograph mechanism is used to amplify the produced motion of the Chebyshev linkage. Pantograph mechanisms, which include the normal and skew configuration in 2D and 3D respectively, are widely used in walking mechanisms because of their characteristics, as pointed out in Ref. [1]. Similar leg mechanisms are also used in the prototypes that have been built at LARM [13] and in the walking chair that has been built in the Tokyo Institute of Technology [10].

Therefore, in this paper we have proposed a single DOF leg mechanism consisting of a Chebyshev four-bar linkage *LEDCB* and a pantograph mechanism *PGBHIA*, as shown in Fig. 2.

The Chebyshev mechanism *LEDCB* can generate an ovoid curve for the point *B*. The crank is *LE*, the rocker is link *CD*, and the coupler triangle is link *EDB*. Joints at *L*, *C*, and *P* are fixed on the body of the biped robot. The offsets *a*, *p*, and *h* between them will greatly influence the trajectory shape of point *A*. The pantograph mechanism *PGBHIA* is used to amplify the input trajectory of point *B* into output trajectory with the same shape at point *A*. In particularly, unlike the traditional design solution, the point *P* is fixed on the body of the robot instead of the point *B* in order to have a more compact robust design. However, drawbacks will exist and in this work the aim is to maintain them within certain limits. The amplify ratio of the pantograph mechanism depends on the length of link *HI* and link *IA* or the ratio of *PA* and *PB* [1].

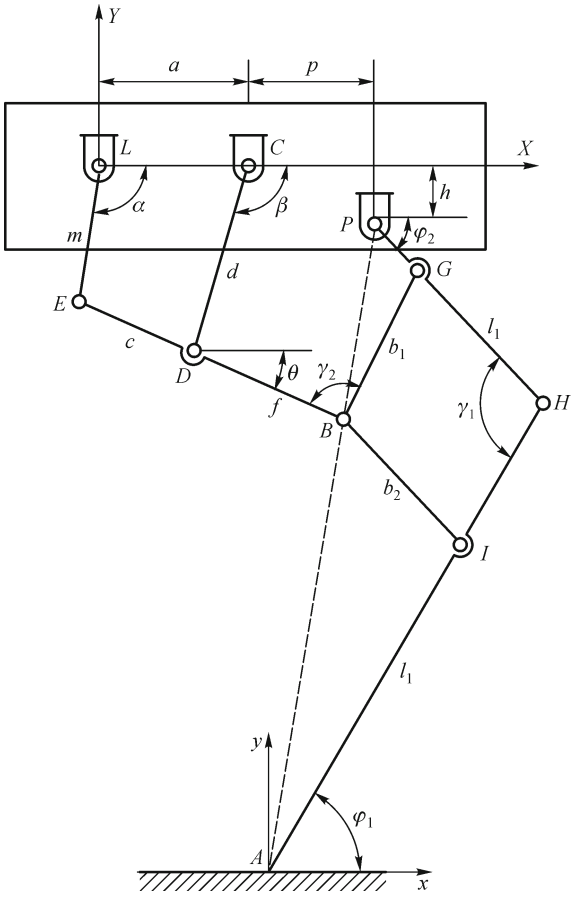

Fig. 2 Kinematic scheme of the proposed single DOF Chebyshev-Pantograph leg mechanism

3 Kinematic analysis

A kinematic analysis has been carried out in order to evaluate the operation performance of the proposed leg mechanism. Actually, the pantograph mechanism amplifies the input motion that is produced by the Chebyshev linkage, as well as the parameters *p* and *h* affect the location and shape of the generated ovoid curve. A kinematic study can be carried out separately in two parts, namely for the Chebyshev four-bar linkage and the pantograph mechanism.

3.1 Kinematic study of Chebyshev four-bar linkage

A scheme of the Chebyshev four-bar linkage *LEDCB* with design parameters is shown in Fig. 2. When the crank *LE* rotates around the point *L* an output ovoid curve can be obtained by point *B*. Assuming a reference frame *XY* fixed at point *L* with *X* axis laying along in the direction of straight line *LC*, it is possible to formulate the coordinates of point *B* as a function of input crank angle α in the form [23],

$$x_B = m\cos\alpha + (c+f)\cos\theta,$$

$$y_B = -m\sin\alpha - (c+f)\sin\theta, \tag{1}$$

where

$$\theta = 2\tan^{-1}\left(\frac{\sin\alpha - (\sin^2\alpha + B^2 - D^2)^{1/2}}{B+D}\right), \tag{2}$$

and

$$B = \cos\alpha - \frac{a}{m},$$

$$C = \frac{a^2 + m^2 - c^2 + d^2}{2md} - \frac{a}{d}\cos\alpha,$$

$$D = \frac{a}{c}\cos\alpha - \frac{a^2 + m^2 - c^2 + d^2}{2mc}. \tag{3}$$

The five design parameters *a*, *m*, *c*, *d*, and *f* characterize the Chebyshev four-bar linkage. A numerical simulation can be carried out by using Eqs. (1)–(3) with proper value

of the design parameters.

3.2 Kinematic study of the pantograph mechanism

The pantograph mechanism PGBHIA with design parameters is shown in Fig. 2. The point P is fixed and point B is connected to the output motion that is obtained by the Chebyshev linkage. The transmission angles γ_1 and γ_2 are important parameters for mechanism efficiency. A good performance can be ensured when $|\gamma_i - 90^\circ| < 40^\circ$ ($i = 1, 2$) according to practice rules for linkages as reported in Ref. [16].

Referring to the scheme in Fig. 2, kinematic equations of the pantograph mechanism can be formulated after some algebraic manipulation in the form [23]:

$$\varphi_1 = 2\tan^{-1}\frac{1-\sqrt{1+k_1^2-k_2^2}}{k_1-k_2},$$

$$\varphi_2 = 2\tan^{-1}\frac{1-\sqrt{1+k_2^2-k_4^2}}{k_3-k_4}, \quad (4)$$

with

$$k_1 = \frac{x_B-p}{y_B-h},$$

$$k_2 = \frac{b_1^2+y_B^2+x_B^2-(l_2-b_2)^2+p^2+h^2-2px_B\text{-}2hy_B}{2b_1(y_B-h)},$$

$$k_3 = \frac{p-x_B}{y_B-h},$$

$$k_4 = \frac{-b_1^2+y_B^2+x_B^2+(l_2-b_2)+p^2+h^2-2px_B-2hy_B}{2(l_2-b_2)(y_B-h)}. \quad (5)$$

Consequently, from Fig. 2 transmission angles γ_1 and γ_2 can be evaluated as $\gamma_1 = \varphi_1 + \varphi_2$ and $\gamma_2 = \pi - \theta - \varphi_1$, respectively. The coordinates of point A can be given as

$$x_A = x_B + b_2\cos\varphi_2 - (l_1-b_1)\cos\varphi_1,$$

$$y_A = y_B - b_2\sin\varphi_2 - (l_1-b_1)\sin\varphi_1. \quad (6)$$

The velocity of point A can be obtained by the derivatives of Eq. (6) and the acceleration of point A can be computed through a further derivative.

By using Eq. (4), the transmission angles γ_1 and γ_2 can be computed to check the practical feasibility of the proposed mechanism. By using velocity and acceleration analysis for the generated ovoid curve, kinematic performance of the proposed leg mechanism can be evaluated.

4 Simulation results

Numerical simulations have been used both to check the operation feasibility and to characterized the walking performance of the proposed leg mechanism design. A simulation program has been developed in the MATLAB environment to study the kinematic performance of the proposed leg mechanism, as well as the feasible walking ability of the single DOF biped robot. Design parameters of the simulated leg mechanism are listed in Table 1.

When the input crank LE rotates around point L with a constant speed, the motion trajectories of point A and point B can be obtained in the form of ovoid curves as shown in Fig. 3. A scheme of the zoomed view of the ovoid curve in Fig. 3 is shown in Fig. 4 in which four characteristic angles of the input crank actuation are indicated. The dimension of the ovoid curve is characterized by the length L and height H.

The generated ovoid curve is composed of an approximate straight-line and a curved segment with a symmetrical shape. The straight-line segment starts at the actuation angle $\alpha = 90^\circ$ and ends at $\alpha = 270^\circ$. Actually, during this 180° interval the leg mechanism is in the non-propelling phase and it swings from rear to forth. During the next 180° interval the actuation angle goes from $\alpha = 270^\circ$ to $\alpha = 90^\circ$ corresponding to the coupler curve segment. In this period, the foot grasps the ground and the leg mechanism is in the propelling phase. The leg mechanism is in a almost stretched configuration when $\alpha = 0^\circ$ just as the leg scheme shows in Fig. 3.

In Fig. 5, the right leg is indicated with solid line as in contact with the ground and the crank actuation angle is at $\alpha = 0^\circ$, the left leg is indicated with dashed line when the crank at angle $\alpha = 180^\circ$ and it swings from rear to forth. The trajectories of points A and point B are also plotted as related to the non-propelling phase. It is noted that at the beginning and the end of the trajectory, the density of the points are higher than in the middle segment. Since the time periods are the same between each plotted points, the velocity of the swinging leg mechanism in the middle is

Table 1 Design parameters of a prototype leg mechanism at LARM with structure of Fig. 2

a	b	c	d	h	m
50	20	62.5	62.5	30	25
f	p	l_1	l_2	b_1	b_2
62.5	30	300	200	75	150

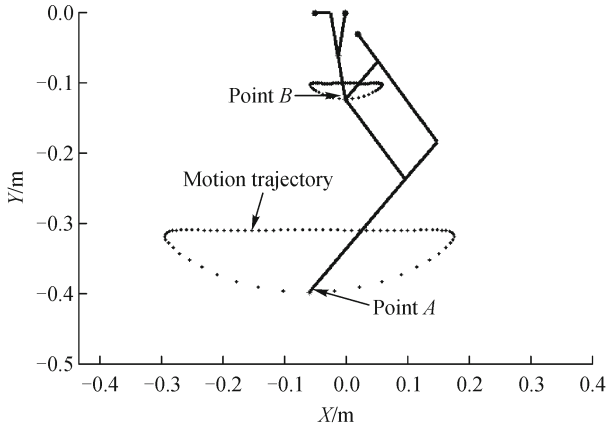

Fig. 3 Computed trajectories of points A and B in a full cycle crank operation

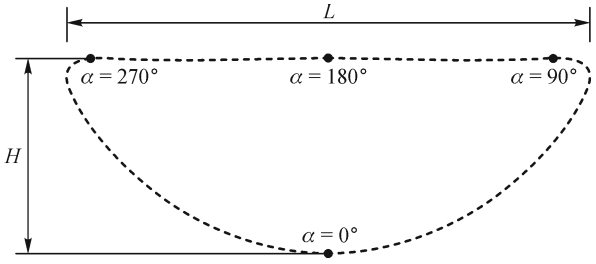

Fig. 4 Characteristics point of the trajectory of point A in Fig. 3

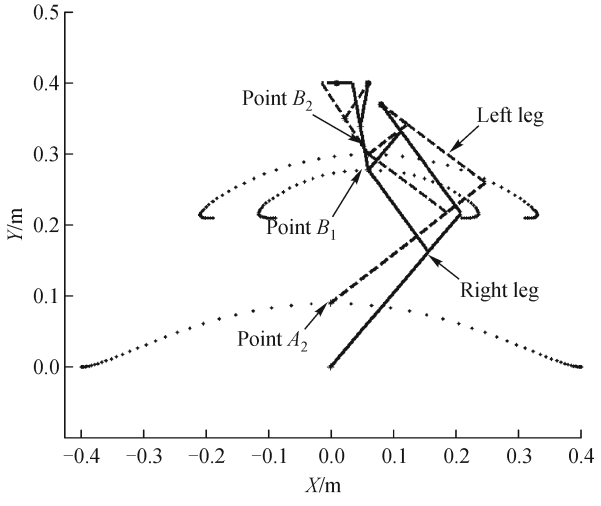

Fig. 5 Simulation results for trajectories of the leg mechanisms during biped walking

higher than that at the start and end of one step.

A scheme of the biped motion and the trajectories of critical points are shown in Fig. 6. Referring to Fig. 6(a), when the leg mechanism is in a non-propelling phase, it swings from rear to forth and the supporting leg propels the body forward. The swinging leg mechanism has a relative

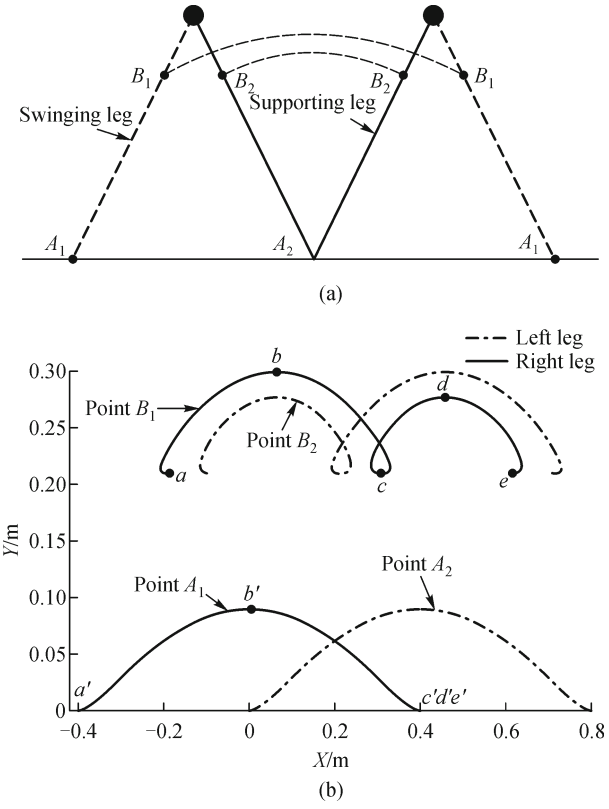

Fig. 6 A characterization of a full cycle of biped walking gait. (a) Scheme of the leg motion; (b) computed trajectories of points A_1, A_2, B_1, and B_2

swing motion with respect to the supporting leg mechanism. Therefore, the velocity of point B_1 in a non-propelling phase with respect to the global inertial frame is larger than that during a supporting phase. This is the reason why the size of curve *a*-*b*-*c* is larger than that the size of curve *c*-*d*-*e* in Fig. 6(b) even if the Chebyshev mechanisms produce the motion with only 180° phase differences at the points B_1 and B_2.

Figure 6(b) shows the trajectories of points A_1, A_2, B_1, and B_2 in a biped walking gait. The trajectories are plotted with solid lines for the right leg mechanism and with dashed lines for the left leg mechanism, respectively. The motion sequences of points B_1 and A_1 are indicated with alphabet letters from *a* to *e* and *a*' to *e*', respectively. In Fig. 6(b), the trajectory segments *a*-*b*-*c* of point B_1 and *a*'-*b*'-*c*' of point A_1 are produced by the right leg mechanism while it swings from rear to forth. The trajectory segments *c*-*d*-*e* is produced while the right leg is in contact with the ground. Correspondingly, *c*', *d*', and *e*' are at the same point. The trajectories of points A_2 and B_2 for left leg mechanism are similar but have 180° differences with respect to the right leg mechanism. There are small circles in the trajectories of point B_1 and point B_2 during the transition of the two walking phases. This happens because there is a short period of time during which both of the legs

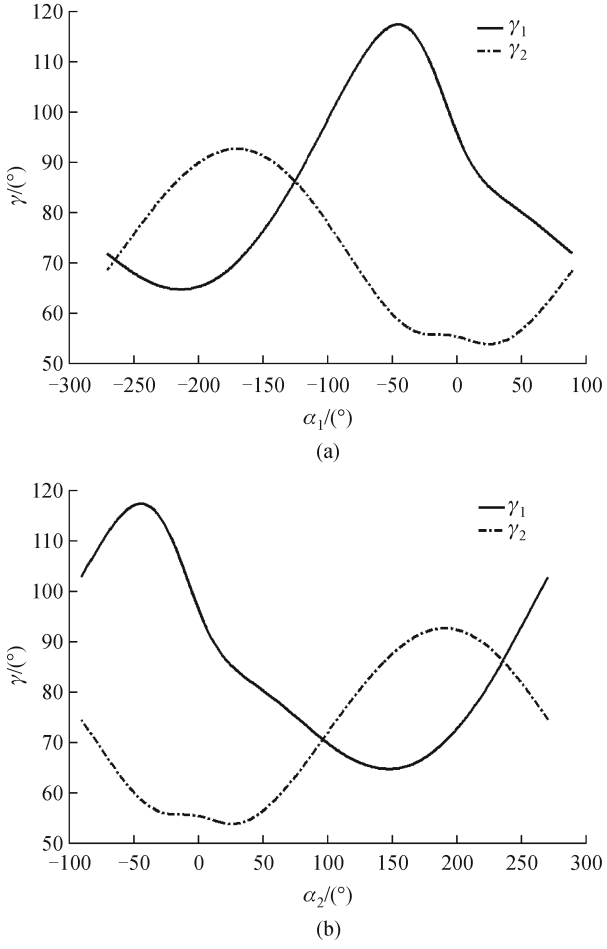

Fig. 7 The transmission angles γ_1 and γ_2 as function of the input crank angles α_1 and α_2. (a) In the right leg mechanism; (b) in the left leg mechanism

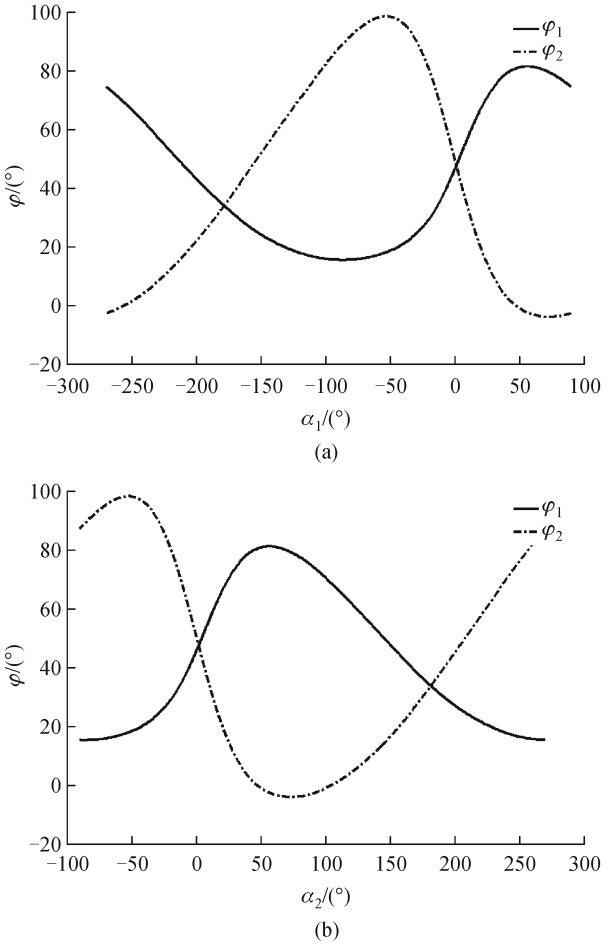

Fig. 8 Angles φ_1 and φ_2 as function of the input crank angles α_1 and α_2. (a) In the right leg mechanism; (b) in the left leg mechanism

are in contact with the ground and a sliding back motion is obtained for the body motion of the biped robot.

Figure 7 shows plots of the computed transmission angles γ_1 and γ_2 of the two leg mechanisms as function of the input crank angles α_1 and α_2, respectively. The value of the transmission angles are computed between 50º and 120º. The transmission angles shows a 180º time differences between the right leg mechanism and left leg mechanism. Therefore, the proposed leg mechanism has an efficient and feasible motion transmission capability.

Figure 8 shows the computed plots for angles φ_1 and φ_2 of the two leg mechanisms as function of the input crank angles α_1 and α_2, respectively. φ_1 is the angle between foot and ground, and φ_2 is the angle between the leg mechanism and body of the biped robot as shown in Fig. 2. The value of φ_1 is between 18º and 100º as a good contact with the ground. The value of φ_2 is between -5º and 100º and there is no confliction between the legs and body. Also angles φ_1 and φ_2 have 180º time differences between the right and left leg mechanisms.

The computed walking motion sequences of the single DOF biped robot in a biped walking gait are shown in Figs. 9 and 10. Figure 9 shows the computed motion sequence of the biped robot in sagittal plane and Fig. 10 shows the foot motion sequence in horizontal plane.

In Fig. 9 the dashed line represents the left leg and the solid line represents the right leg. The right foot grasps the ground and the left leg swings in the air. Two configurations are shown in the figure with actuation angle $\alpha_1 = 270°$ and $\alpha_1 = 90°$.

In Fig. 10 the triangles represent the right foot and the rectangles represent the left foot in the horizontal plane. A black circle represents that the foot grasps the ground and the corresponding leg is in the propelling phase, otherwise it represents the foot in the air and the leg is in a non-propelling phase. A logic flowchart of the walking gaits for the biped robot is listed in Fig. 11. The two leg mechanisms operate sequentially in propelling and non-propelling phases to obtain a proper forward motion of the biped robot.

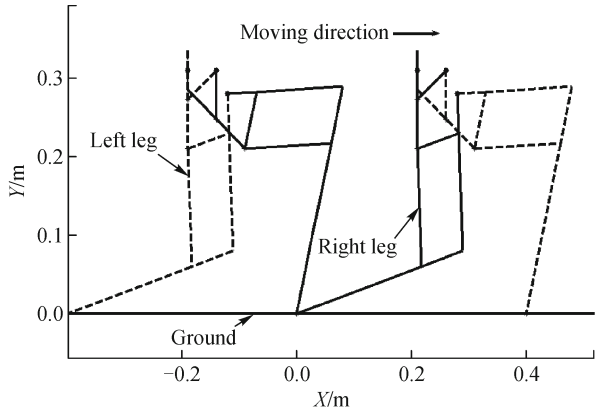

Fig. 9 Motion sequences in sagittal plane when the biped robot walks

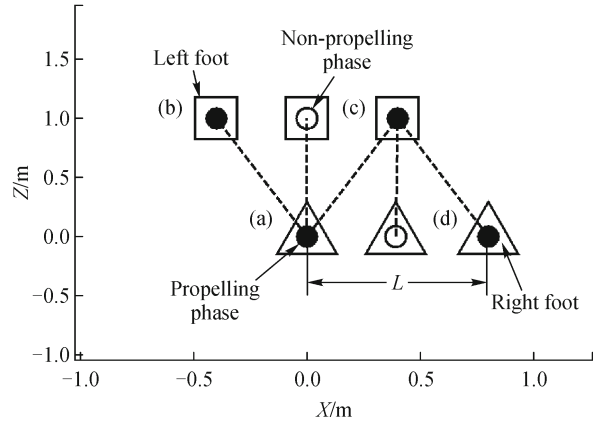

Fig. 10 Motion sequences in horizontal plane when the biped robot walks

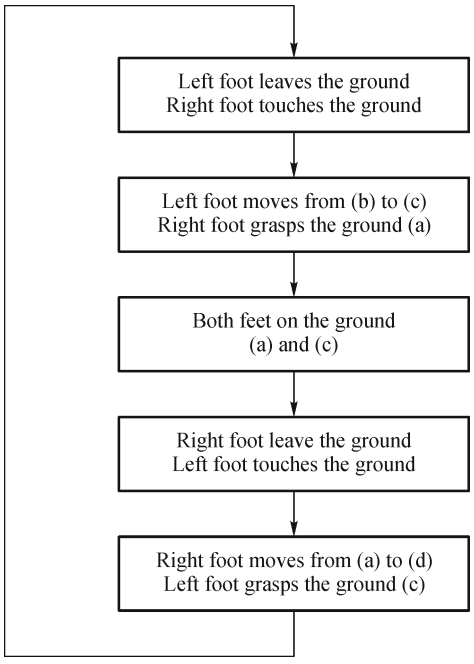

Fig. 11 Flowchart for the walking gait of the biped robot as referring to scheme in Fig. 10

5 A motion study

A motion study has been carried out to evaluate the dynamic operation performance of the proposed leg mechanism. The mass of the linkages are listed in Table 2. The mass center is supposed to be in the center of each linkage. Therefore, center of gravity (COG) of the biped robot can be computed by considering the body mass and mass center of the linkages.

In Fig. 12, the computed trajectory of COG of the biped robot is plotted. The trajectory of COG is a cyclic sinusoid shaped curve in the saggital plane. It reaches the highest point when the supporting leg mechanism is at the most stretched configuration and reaches the lowest point in the double supporting phase of the two legs.

By using the principle of virtual work, the actuation torque of the input crank is equal to the torque which is generated by the gravity force at the supporting foot point. The result is computed as shown in Fig. 13 as function of the input crank angle α_1. The value of the input torque is between 0 and 2.2 N·m. It reaches the maximum value when the crank angle α_1 is at 0º or 180º and the minimum value when the crank angle α_1 is at 90º or 270º. Particularly, the input torque is not continuous during the transition between propelling and non-propelling phases, since the supporting point changes between the feet of the biped robot.

The acceleration of point A is computed by using kinematics equations. Figure 14 shows the computed acceleration values of point A along X and Y axis, respectively. Similarly, Fig. 15 shows the acceleration of point P on the body of the biped robot.

In Fig. 14, the acceleration of point A at the end of leg mechanism is computed between -1 to 10 m/s^2 along X axis and between -10.5 to -3.5 m/s^2 along Y axis. The

Table 2 Mass of a prototype leg mechanism at LARM with structure of Fig. 2 (kg)

m_{LE}	m_{EB}	m_{CD}	m_{Body}
0.025	0.05	0.025	0.15
m_{BI}	m_{PH}	m_{HA}	m_{BG}
0.035	0.08	0.11	0.025

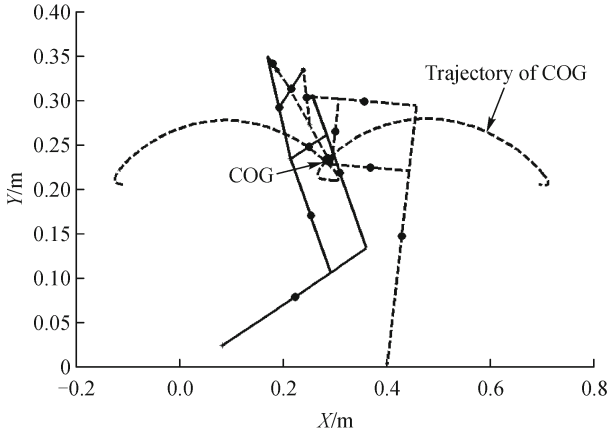

Fig. 12 Computed trajectory of COG of the biped robot

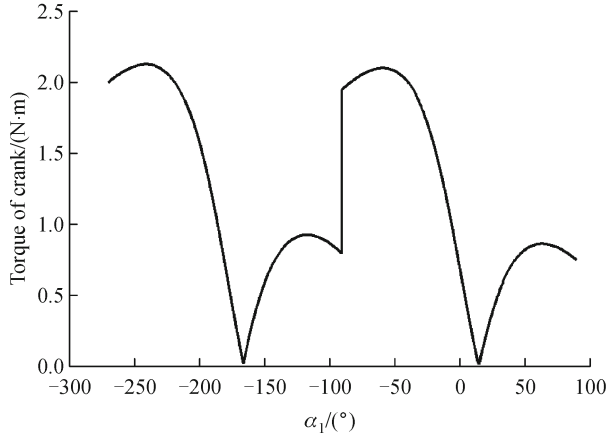

Fig. 13 Computed actuation torque on the crank when the biped robot walks

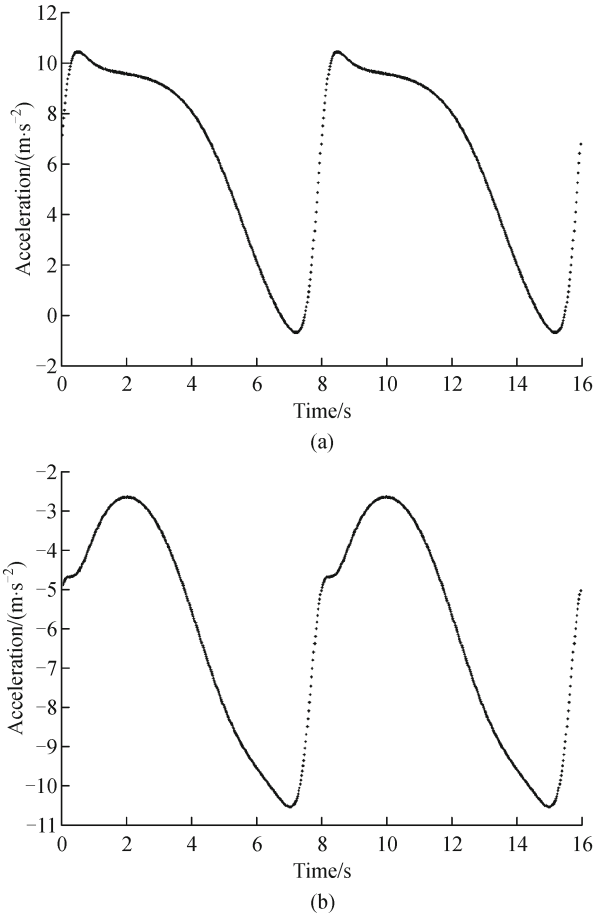

Fig. 14 Computed acceleration of point A during one biped walking gait in Fig. 12. (a) Acceleration along X axis; (b) acceleration along Y axis

acceleration along X axis reaches the maximum value when the input crank angle is at $t = 0.5$ s ($\alpha = 20°$) and the minimum value when it is at $t = 7.3$ s ($\alpha = 325°$).

In Fig. 15, the acceleration at point P is computed between -2.3 and 9 m/s^2 along X axis and between -10.2 and -0.2 m/s^2 along Y axis. The acceleration in X axis reaches the maximum value when one leg mechanism is in the middle of supporting phase and acceleration in Y axis reaches the minimum value, correspondingly. The acceleration in X axis reaches the minimum value during the transition phase of leg mechanisms and the negative value shows that the biped robot in a double supporting phase and produces a back sliding motion.

6 Experimental tests

A prototype of single DOF biped robot has been built at LARM to evaluate the practical operation feasibility of the proposed leg mechanism. The design parameters are those simulation parameters listed in Tables 1 and 2.

Figure 16 shows a prototype of single DOF biped robot fixed on a supporting test bed. It consists of two leg mechanisms with the proposed design. The leg mechanisms are connected to the body with simple revolute joints and they are actuated by only one DC motor through a gear box. The actuated crank angles of the two leg mechanisms are 180° synchronized. Therefore, when one leg mechanism is in non-propelling phase the other leg mechanism is in propelling phase and vice versa. A big U shaped foot is connected at the end of each leg mechanism with a revolute joint equipped with a torsion spring. The torsion spring makes the foot contact with the ground properly so that it has adaptability to rough terrain and as well as the walking stability of the biped robot is improved.

During the experimental tests accelerometers are attached at point A' at the end of leg mechanism as indicated in Fig. 16. In order to evaluate the walking performances, an accelerometer is also attached on the

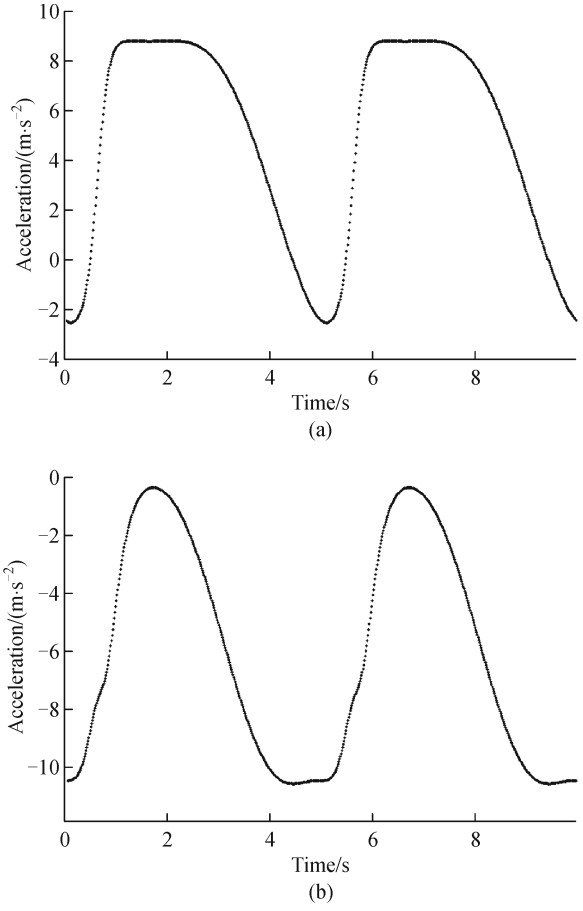

Fig. 15 Computed acceleration of point P during one biped walking gait in Fig. 12. (a) Acceleration along X axis; (b) acceleration along Y axis

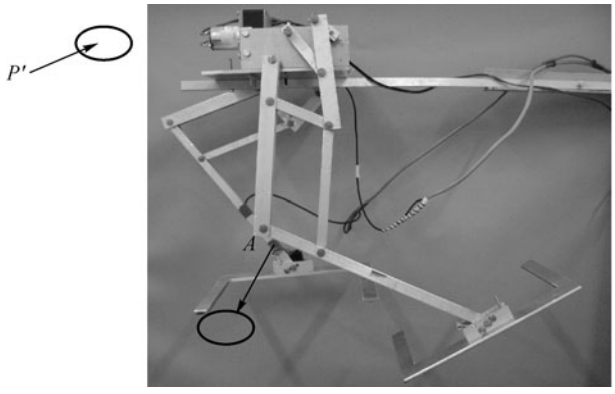

Fig. 16 A prototype of a single DOF biped robot with two proposed leg mechanisms at LARM

body of the robot at point P' as indicated in Fig. 16. The body acceleration has been measured when the biped robot walks on the ground. The output signals of the accelerometers are acquired through a NI 6024E card in a PC. Data are handled in the LABVIEW environment.

The used accelerometers in the lab test can only measure the acceleration signals along one axis, which is orthogonal the surface of the accelerometer. Therefore, the acquired acceleration signals are with respect to the reference frame $X'Y'$ which is fixed on the end of the foot, as shown in Fig. 17. A global inertial coordinate frame XY is fixed on the ground. Accelerometers can only measure the acceleration signals along X' axis. Since the accelerometers have been attached on the feet or on the body a coordinate transformation has been computed, in order to obtain the acceleration values with respect to the global inertial coordinate system XY.

The rotation matrix between XY and $X'Y'$ is

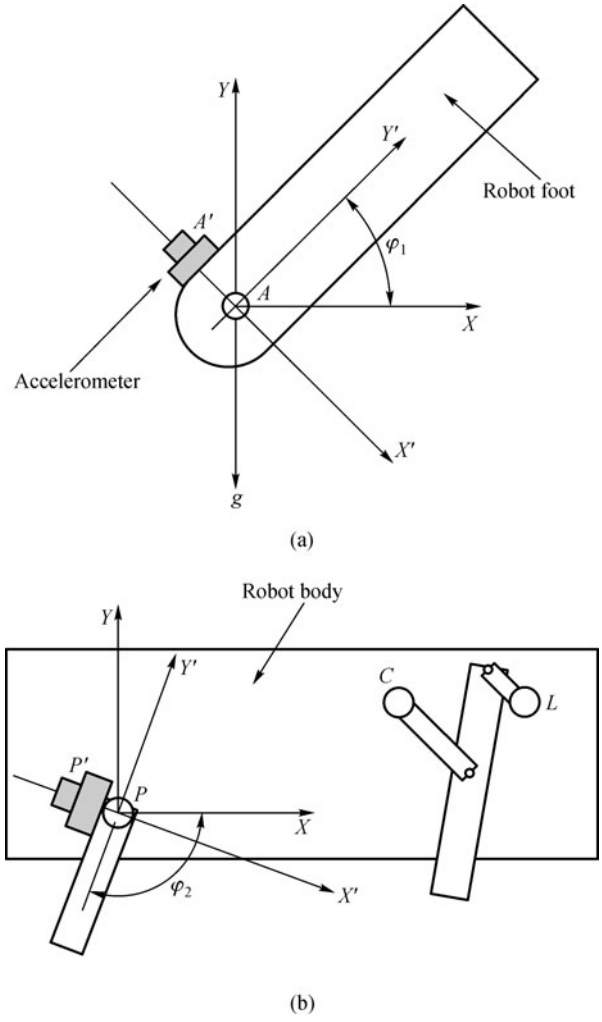

Fig. 17 Position of accelerometers and reference frames in Fig. 16 during experimental tests. (a) Accelerometer at point A' at the end of foot; (b) accelerometers at point P' on the body

$$\boldsymbol{R} = \begin{bmatrix} \sin\varphi & -\cos\varphi & 0 \\ \cos\varphi & \sin\varphi & 0 \\ 0 & 0 & 1 \end{bmatrix}. \quad (7)$$

Thus, acceleration along X axis can be expressed as

$$a'_A = Ra_A,\ g' = Rg,\ a'_A = -a_A - g'. \quad (8)$$

where a'_A and g' represent the foot acceleration and gravity acceleration with respect to reference frame $X'Y'$.

Results of experimental tests are reported in Figs. 18 and 19. In Fig. 18 the acceleration components of the point A' are plotted as function of time when the leg mechanism operates on a test bed. Figure 19 shows the measured acceleration at the point P' on the robot body when the prototype walks on the ground.

The time of one period in Fig. 18 is twice as compared with the period in Fig. 19. This is because in a full biped walk gait the body of the robot has twice up and down motion in the saggital plane. The acceleration at point A' is between 0 and 9 m/s^2 along X axis. Along Y axis it is between -10 and -2.5 m/s^2. The acceleration at point P' is between -2.2 and 6 m/s^2 along X axis. Along Y axis it is between -10.5 and -6 m/s^2.

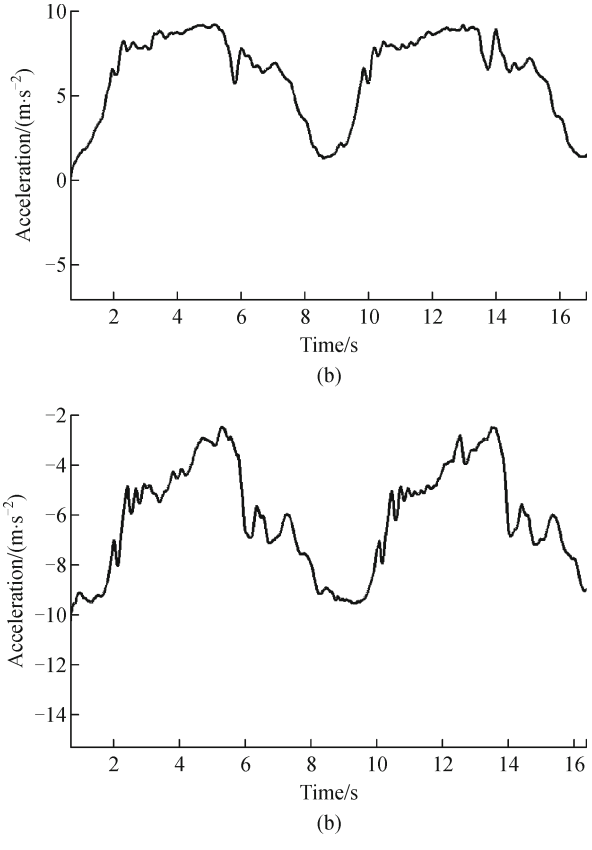

Fig. 18 Measured accelerations at point A' at the end of foot during experimental tests. (a) Acceleration along X axis; (b) acceleration along Y axis

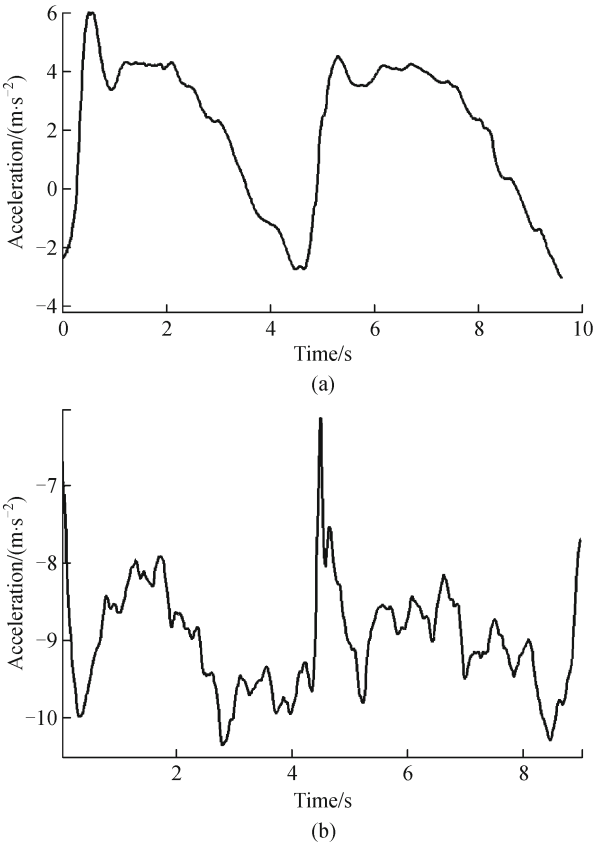

Fig. 19 Measured accelerations at point P' on the body during experimental tests. (a) Acceleration along X axis; (b) acceleration along Y axis

In order to evaluate the practical operation performance of the built prototype, measured accelerations and computed accelerations can be usefully compared. It can be noted that the experiment results confirm the simulation results as they are similar and comparable. However, because of the mechanism clearance, vibration, backlash, and also measuring errors, experiment results are no coincident with the simulation results.

Figure 20 shows the snapshots of the walking sequence of the biped robot during a lab test. Laboratory experimental test results have shown feasible operation of the proposed leg mechanism in this biped robot although it dose not walk properly as outlined in Fig. 20. As shown in Fig. 19(a), the maximum acceleration of the body in X axis is about 6 m/s^2 and varies in a large region that means at each step the robot rush forward and its foot hits the ground heavily. Experiment videos show that the biped robot walks just like a "drunk-man". This is not an efficient and practical feasible walking gait. Additionally, step length L is almost equal to the dimension of the leg mechanism this decreases the walking stability of the biped robot. The

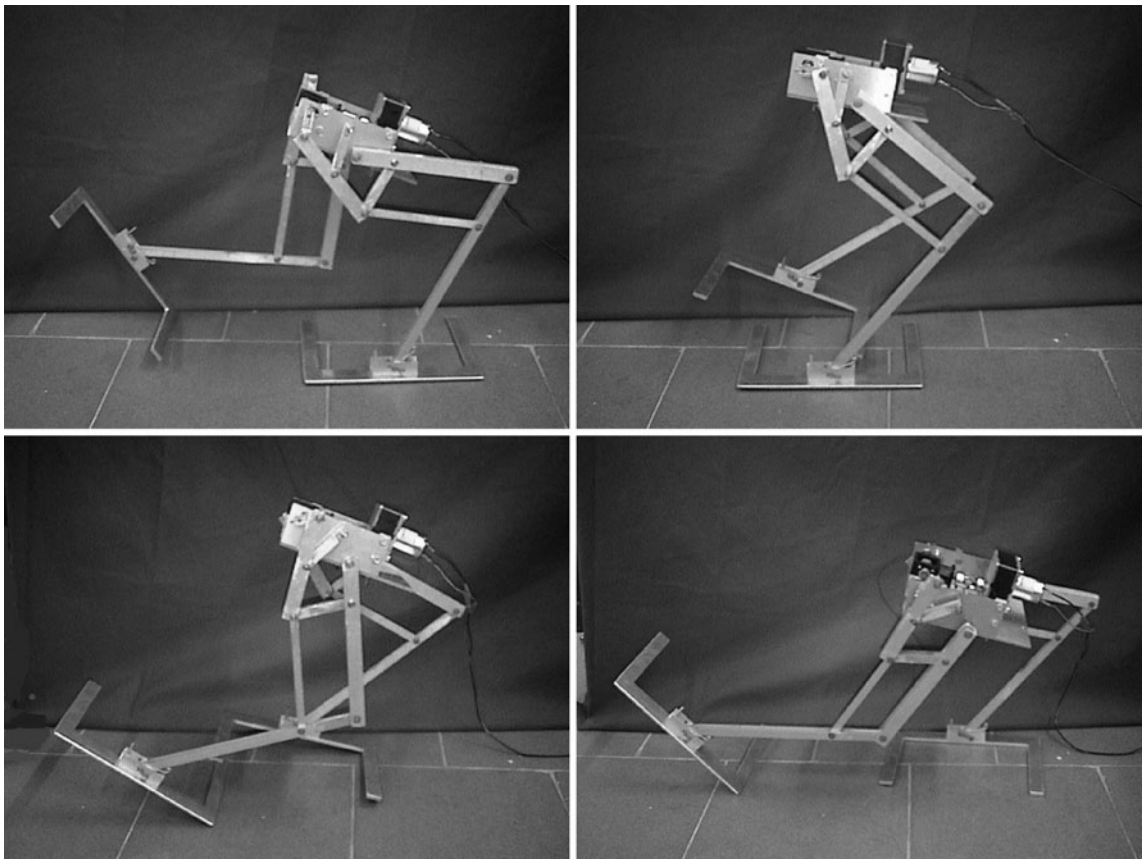

Fig. 20 Snapshots of the walking sequences by the LARM prototype in a lab test

COG of the biped robot sometimes goes out of support polygon of the feet and the biped robot lost balance.

7 Parametric study for design solution

An optimized design of the leg mechanism can achieve an efficient and practical feasible walking gait. In this section, a parametric study has been proposed to characterize the operation performance of the proposed single DOF biped robot as function of its design parameters. Actually, the lengths of the linkages determine a proper shape and size of the generated ovoid curve produced by the Chebyshev linkage and the amplification ration of the pantograph mechanism as shown in Fig. 2. Therefore, only three parameters a, p, and h can be considered as significant design variables.

In Fig. 21, results of the parametric study are plotted as function of parameter a.

By increasing the value of parameter a, size of the ovoid curve is decreased in X axis and is increased in Y axis as shown in Fig. 21(a). Particularly, the ovoid curve with an approximately straight line segment is obtained when a = 0.05 m. Figure 21(b) shows the corresponding trajectories of COG and the feet of swinging leg when the other leg mechanism is in contact with the ground. The step length L decreases and step height H increases as function of the value of parameter a, as shown in Fig. 21(b).

In Fig. 22, results of parametric study are plotted as function of parameter p. In Fig. 22(a), by varying parameter p the ovoid curve generated at point A has only displacements along X without change of the step length L and step height H. The COG of the biped robot has corresponding displacements along X axis. Similarly, by varying parameter h, the COG of the biped robot has displacements along Y axis as shown in Fig. 23. Therefore, the position of point P determines the location of the ovoid curve without any shape change. Correspondingly, the location of COG of the biped robot can be as function of the position of point P since the mass center of the leg mechanism varies correspondingly.

The parametric study have analyzed the shape of the generated ovoid curve as function of three parameters a, p, and h. The parametric study whose main results are shown in Figs. 21–23 has been aimed to check the motion possibility and design sensitivity of the proposed leg mechanism. Interesting outputs of the parametric study can be considered in the following aspects:

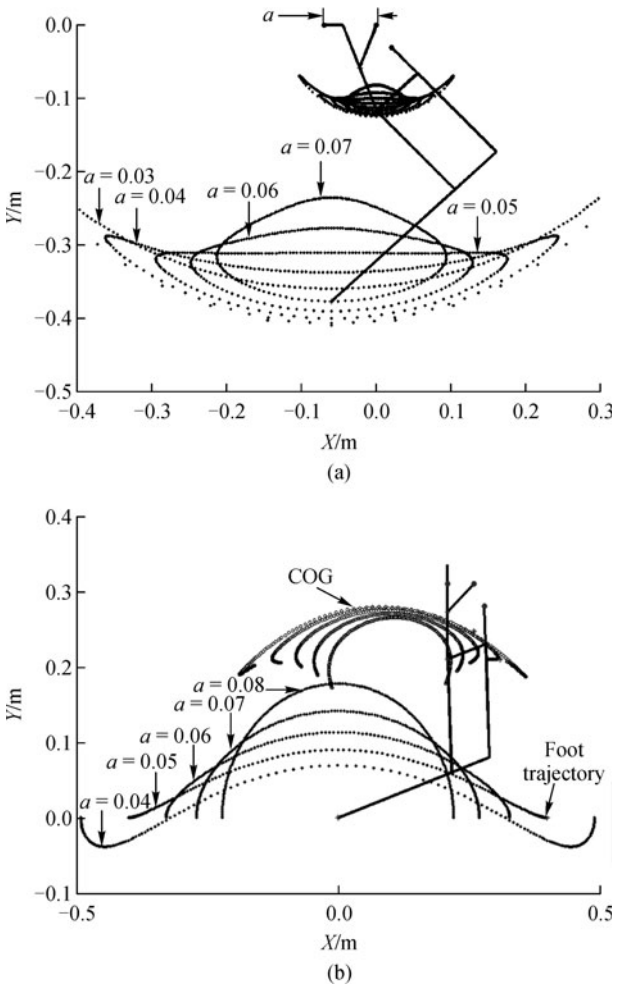

Fig. 21 A parametric study of the leg mechanism as function of parameter a in Fig. 2. (a) Generated ovoid curves at point *A*; (b) trajectories of COG and foot trajectory of the swinging leg

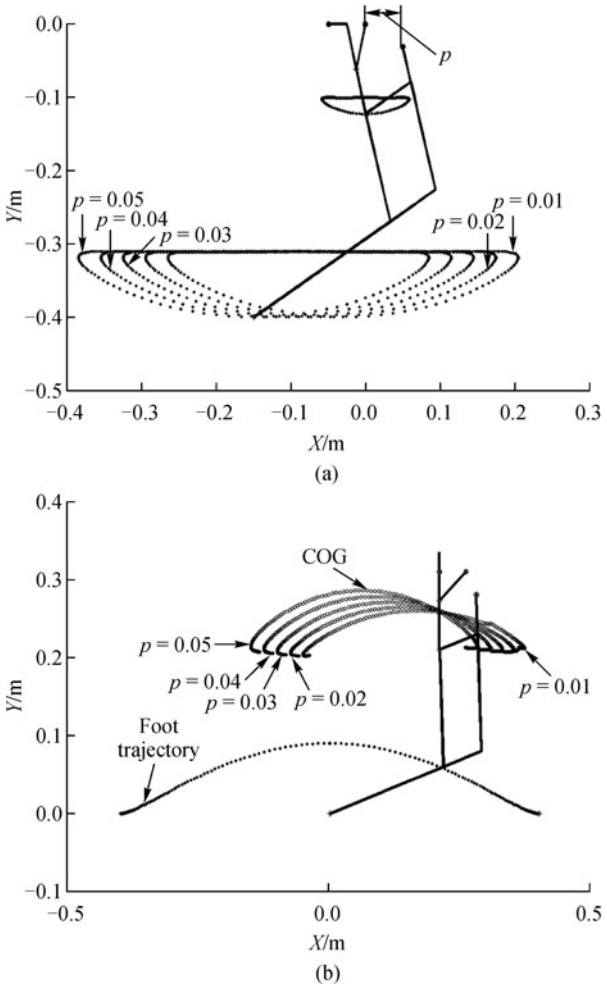

Fig. 22 A parametric study of the biped robot as function of parameter *p* in Fig. 2. (a) Generated ovoid curves at point *A*; (b) trajectories of COG and foot point of swinging leg

1) The kinematic behaviour in terms of point trajectories is robust and well suited to walking tasks.

2) Variations of main design parameters do not affect considerably main characteristics of the walking operation.

3) The size of the walking step can be modified by changing the parameter a only.

4) The size of height of swinging leg motion can be modified by changing the parameter *h* only.

Main drawbacks of the proposed solution can be recognized in a fixed foot trajectory capability and linkage size of the leg mechanisms. When the leg mechanism is determined, the foot trajectory cannot be changed for step flexibility or obstacle overpassing so that the solution does not show possibility to adapt to variety of environment scenario. The size of the combined two linkages make the overall mechanical design more encumbering than a pure anthropomorphic two-link design.

Therefore, an optimized mechanical design for leg mechanism and an efficient walking gait for minimizing input crank torque can be determined by selecting proper design parameters.

8 Conclusions

In this paper, an operation analysis of a Chebyshev-Pantograph leg mechanism is presented to characterize its design and operation. Kinematic equations of the proposed leg mechanism are formulated for a computer oriented simulation in the MATLAB environment. Simulation results show a feasible performance of proposed leg mechanism for biped walking. Experimental tests have been carried out by using the prototype that has been built at the LARM laboratory. Simulation and experiments results show the practical feasible operation performance of the leg mechanism in a single DOF biped robot. A

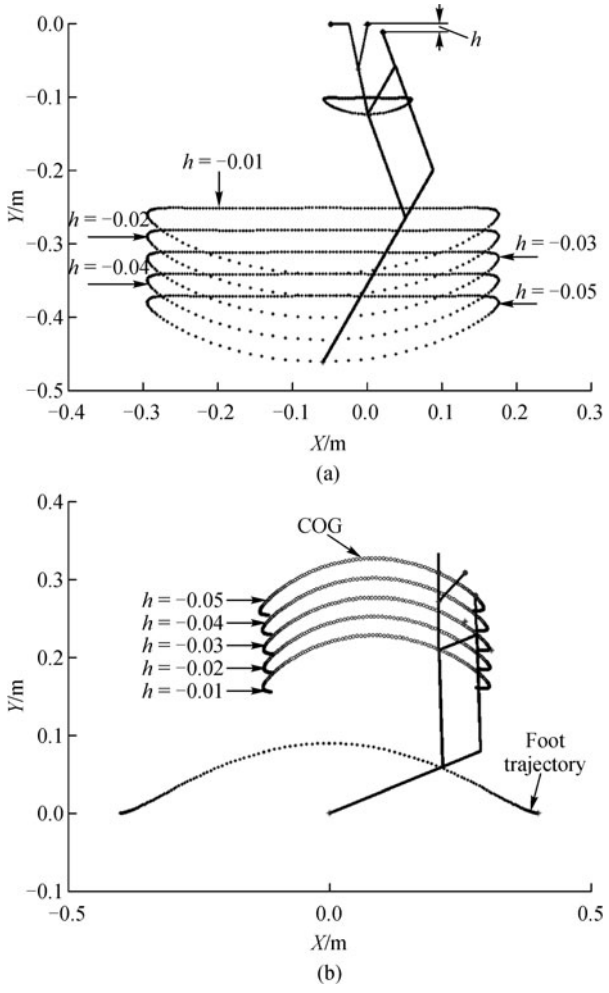

Fig. 23 A parametric study of the biped robot as function of parameter h in Fig. 2. (a) Generated ovoid curves at point A; (b) trajectories of COG and foot point of swinging leg

parametric study has been developed to look for an optimized mechanical design and to determine an energy efficient walking gait.

Acknowledgements The first author is supported by the Chinese Scholarship Council (CSC) for his PhD study and research at LARM in the University of Cassino, Italy for the years 2008–2011.

References

1. Song S M, Waldron K J. Machines That Walk: The Adaptive Suspension Vehicle. Cambridge MA: The MIT Press, 1988
2. Carbone G, Ceccarelli M. Legged robotic systems. Cutting Edge Robotics, 2005, 553–576
3. Kanehiro F, Kajita S, Hirukawa H, Kawasaki T, Hirata M, Akachi K, Isozumi T. Humanoid robot HRP-2. In: Proceedings of the 2004 IEEE International Conference on Robotics and Automation, New Orleans, USA, 2004, 1083–1090
4. Omer A M M, Ogura Y, Kondo H, Morishima A, Carbone G, Ceccarelli M, Hun-ok L, Takanishi A. Development of a humanoid robot having 2-DOF waist and 2-DOF trunk. In: Proceedings of the 5th IEEE-RAS International Conference on Humanoid Robots, Tsukuba, Japan, 2005, 333–338
5. Sakagami Y, Watanabe R, Aoyama C, Matsunaga S, Higaki N, Fujimura K. The intelligent ASIMO: System overview and integration. In: Proceedings of the IEEE/RSJ International Conference on Intelligent Robots and Systems, Switzerland, 2002, 2478–2483
6. Yan H S. Reconstruction Designs of Lost Ancient Chinese Machinery. Dordrecht: Springer, 2007, 269–277
7. Artobolevsky I I. Mechanisms in Modern Engineering Design: A Handbook for Engineers, Designers, and Inventors. Moscow: Mir Publisher, 1979
8. Funabashi H, Horie M, Tachiya H, Tanio S. A synthesis of robotic pantograph mechanisms based on working spaces and static characteristics charts, JSME International Journal Series III, 1991, 34(2): 239–244
9. Shieh W B, Tsai L W, Azarm S. Design and optimization of a one-degree-of-freedom six-bar leg mechanism for a walking machine. Journal of Robotic Systems, 1997, 14(12): 871–880
10. Takeda Y, Higuchi M, Funabashi H, Oki Y, Shimizu K. Development of a walking chair (Fundamental investigations for realizing a practical walking chair). In: Proceedings of the 4th International Conference on Climbing and Walking Robots, Karlsruhe, Germany, 2001, 1037–1044
11. Wu Y F, Nakamura H, Takeda Y, Higuchi M, Sugimoto K. Development of a power assist system of a walking chair based on human arm characteristics. Journal of Advanced Mechanical Design, Systems and Manufacturing, 2007, 1(1): 141–154
12. Ottaviano E, Lanni C, Ceccarelli M. Numerical and experimental analysis of a pantograph-leg with a fully-rotative actuating mechanism. In: Proceedings of the 11th world Congress in Mechanism and Machine Science, Tianjin, China, 2004
13. Ceccarelli M, Figliolini G, Lanni C, Ottaviano E. A study of feasibility for rickshaw type mobile robot. In: Proceedings of the 26th Annual Conference on Industrial Electronics Society, Nagoya, Japan, 2000, 2: 924–926
14. Rodriguez N E N. Anthropomorphic design and operation of a new low-cost humanoid robot. Dissertation for the Doctoral Degree. Cassino: University of Cassino, 2007
15. Mcmahon T A. Mechanics of locomotion. The International Journal of Robotics Research, 1984, 3(2): 4–16
16. Hartenberg R S, Denavit J. Kinematics Synthesis of Linkages. New York: McGraw-Hill, 1964
17. Uicker J J, Pennock G R, Shigley E. Theory of Machines and Mechanisms. 3rd ed. New York: Oxford University Press, 2003
18. Shieh W B. Design and optimization of planar leg mechanisms featuring symmetrical foot-point paths. Dissertation for the Doctoral Degree. Maryland: University of Maryland, 1996
19. Funabashi H. Adjustable mechanism with variable crank length. Bulletin of the Japan Society of Mechanical Engineers, 1985, 51 (470): 2737–2743
20. Funabashi H, Ogawa K, Gotoh Y, Kojima F. Synthesis of leg-mechanism of biped walking machine: Part I, synthesis of ankle-

path-generator. Bulletin of the Japan Society of Mechanical Engineers, 1985, 28(237): 537–543

21. Funabashi H, Ogawa K, Honda I, Iwatsuki N. Synthesis of leg-mechanism of biped walking machine: Part II, synthesis of foot-driving mechanism. Bulletin of the Japan Society of Mechanical Engineers, 1985, 28(237): 544–549
22. Mehdigholi H, Akbarnejad S. Optimization of Watt's six-bar linkage to generate straight and parallel leg motion. Journal of Humanoids, 2008, 1(1):11–16
23. Ottaviano E, Ceccarelli M, Tavolieri C. Kinematic and dynamic analyses of a pantograph-leg for a biped walking machine. Climbing and Walking Robots, 2005, 561–568